High Standard One-Loop Potential Clamp Device for Ranvier Nodes

M. ALBERS, K. H. BOHUSLAVIZKI and E. KOPPENHÖFER

Institute of Physiology, University of Kiel, Olshausenstr. 40, 2300 Kiel, Federal Republic of Germany

Abstract. Starting from the observation that using a conventional potential clamp device for membrane current measurements in Ranvier nodes neither the kinetics of sodium currents nor the constant field concept agree satisfactorily with the Hodgkin-Huxley-Frankenhaeuser (HHF)-formalism, an extendend measuring system has been developed. The extensions introduced base largely on physical implications of myelinated nerve fibres which give rise 1. to systematic distortions of any current records at the high frequency end and 2. to current proportional deviations of the membrane potential from desired potential values. In addition, we provided to meet any unwanted current load during membrane current measurements and to push the time resolution of the measuring system to the highest possible value. After having tested thoroughly the new circuitry by appropriate physical methods, from sodium current measurements the following conclusions were drawn: 1. Occasional deviations of sodium current kinetics near the sodium equilibrium potential from the predictions of the HHF-formalism are measurement errors. 2. The constant field formalism holds for sodium currents in the potential range of biological relevance only. 3. Instantaneous sodium current measurements, however, are of unsatisfactory significance because for this kind of experiments the time resolution of the measuring system used might be still too low.

Key words: Ranvier node — Potential clamp — Equipment reliability — Constant field concept — Sodium kinetics

Introduction

In a foregoing paper (Koppenhöfer and Bohuslavizki 1988) the sodium currents in Ranvier nodes were tested in the light of the Hodgkin-Huxley-Frankenhaeuser (HHF) formalism (Frankenhaeuser and Huxley 1964) using the potential clamp device according to Nonner (1969). Considerable differences in both peak values and kinetics of sodium currents as well as in their instantaneous

values from the predictions of the formalism were attributed to the specific measuring device used. In this connexion weighty technical imperfections of the commercially available version of the device used were named: 1. Both accuracy of membrane current measurements and their time resolution are reduced systematically by inevitable destruction of the cable-structure of the axon within the air gap (Sommer et al. 1982). 2. Membrane potential measurements are complicated by considerable current load of the potential measuring internode (Steinmetz 1979; Steinmetz et al. 1980). 3. Any current record is slowed down by low-pass filter properties of the current measuring internode (Schumann et al. 1983). 4. Absence of positive feedback for electronic compensation for the voltage drop across the Schwann cell structures lying in front of the nodal membrane (Berthold and Rydmark 1983 a) causes current proportional deviations of the membrane potential from desired potential values and, moreover, slows down any potential step (Ramón et al. 1975). Consequently, peak value and time course of any current record are also distorted in a characteristic fashion (Koppenhöfer et al. 1984; Zaciu et al. 1981). All these engineering deficiencies obviously reduce the reliability of measured data, in particular as far as fast current components are concerned, e.g. sodium activation kinetics and asymmetrical currents.

When repeating the experiments performed previously with the original version of the potential clamp device according to Nonner (Koppenhöfer and Bohuslavizki 1988) we could show in an exemplary study that the most important technical imperfections of the original version can be successfully minimized. Thus, membrane current measurements can now be performed approximately in the fashion as we claimed before it were actually the case.

Materials and Methods

General. Membrane currents were measured on single potential clamped myelinated nerve fibres of the toad (*Xenopus laevis*). There are indications for the series resistance of Ranvier nodes being smallest provided that the reserve length of the axon under investigation remains largely intact up to the end of measurements. Therefore, starting from nerve bundles showing well preserved spiral bands of *Fontana* (Clarke and Bearn 1972) we followed the dissection procedure outlined by Koppenhöfer and coworkers (1987) which delivered clearly curled thick axons of 23 μm in diameter (median; range 22 to 28 μm, $n = 6$) with barely visible Ranvier nodes.

Absolute membrane potentials were termed E. The holding potential, E_H, was set at $E_H = -80$ mV throughout. Rectangular pulses, U, of either direction were applied which equalled deviations from E_H, V, (Dodge and Frankenhaeuser 1959) provided that the effective electrical resistance working in series with the nodal membrane was negligibly small. Positive test pulses were preceded by negative prepulses of $U_{pp} = -40$ mV and 50 ms duration, thus at the beginning of test pulses the inactivation variable, h, was unity. Membrane current records were corrected for leakage currents automatically, assuming potential independent leakage conductance (Dodge and Frankenhaeuser 1958). Specific currents were calculated from the corresponding output voltages of the

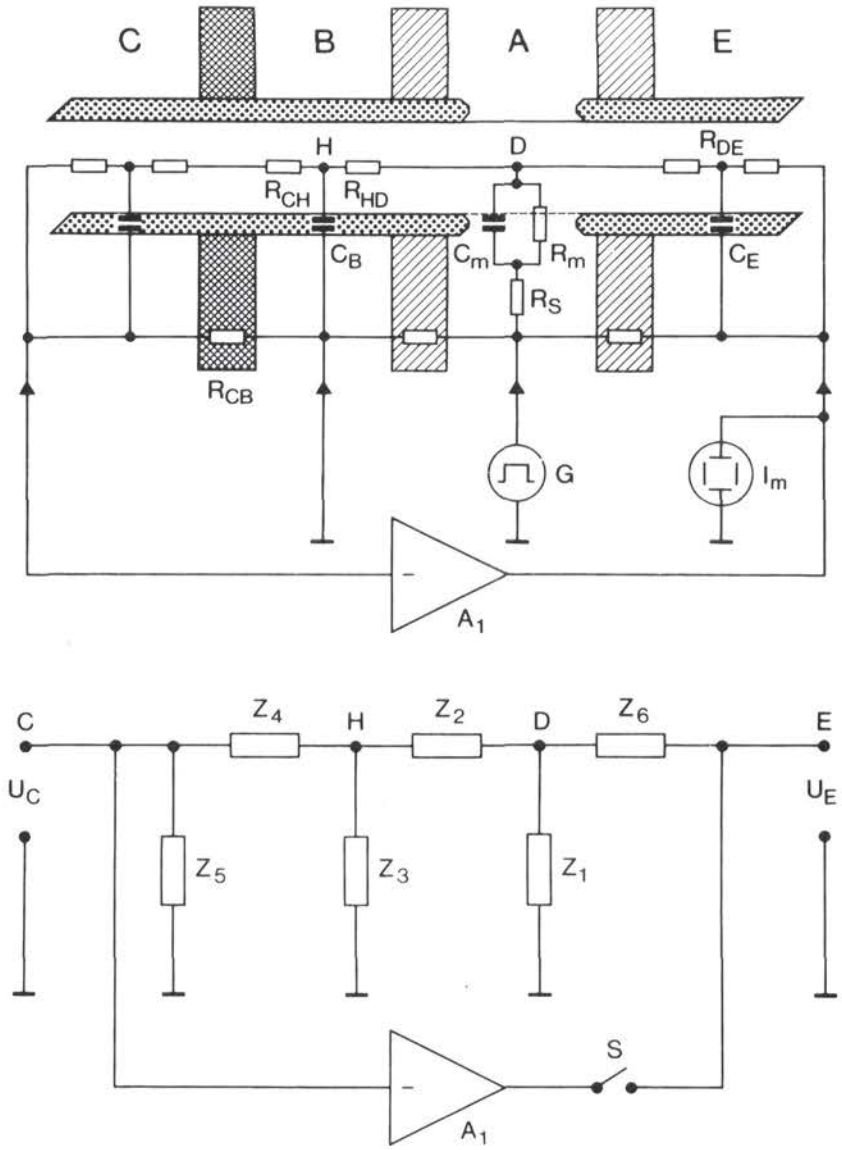

Fig. 1. Schematic diagram of the preparation in the original potential clamp configuration. *Top:* The axon is laid across four fluid pools C, B, A, and E of the recording chamber; the node under investigation is in A. D: point inside the node. Vaseline seals: hatched areas. Air gap: cross-hatched areas. Filled triangles: Ag/AgCl electrodes. A_1: clamp amplifier. G: low impedance pulse generator. I_m: oscilloscope for recording membrane currents. *Bottom:* Equivalent diagram of the open-loop configuration represented by impedances as defined by the respective resistance and capacitances shown above.

clamp amplifier and the fibre dimensions according to the passive standard data of myelinated nerve fibres (Stämpfli and Hille 1976) and filtered to a permissible extent by means of a switchable 4-pole Bessel filter or signal-averaged (see page 420) after being digitized by a 12 Bit A/D converter at a sampling frequency of 250 kHz.

The node under investigation was continuously rinsed by Ringer solution containing (in mmol/l): NaCl 107.0; KCl 2.5; $CaCl_2$ 2.0; N,N-Bis(hydroxyethyl)-2-amino-ethanesulfonic acid/NaOH-buffer (BES) 5.0 (Bethge et al. 1989). The adjacent internodes were cut and immersed in an artificial intracellular fluid containing (in mmol/l): KCl 108.0; NaCl 5.0; BES-buffer 5.0. The temperature was kept at constant values (± 0.5 °C) between 10 and 15 °C and the pH was 7.2 ± 0.1 throughout.

Original circuitry. Both the potential clamp configuration in question and its improved version are tuned one-loop negative feedback measuring systems using extracellular electrodes. A schematic drawing of the original setup is shown in Figure 1 (top). The nerve fibre is mounted and sealed by vaseline (hatched) on the recording chamber, thus connecting four fluid pools C, B, A and E with the node under investigation located in A and the neighbouring nodes being cut. Note the air gap (cross-hatched) between C and B. Any internodal current between C and inside the node (D) flows across the air gap resistance R_{CB} and produces a potential drop. The negative feedback action of the amplifier, A_1, minimizes such a potential drop thus keeping D near ground potential by minimizing any intraaxonal current load. Therefore, provided the voltage drop across the nodal series resistance, R_S, is negligibly small, the potential in A with respect to ground equals the absolute membrane potential E (Wiese and Duchâteau 1984) which can be changed by the pulse generator G. The resulting changes of output voltages of A_1 reflect the membrane currents of the node under investigation provided the high-frequency cut by the current measuring impedance (formed by R_{DE} and C_E) can be tolerated.

Starting from a condensed equivalent diagram of the open loop configuration and composed of impedances, Z, (Fig. 1 below) we derived the transfer function of the axon under investigation, F_N, by U_C/U_E

$$F_N = \frac{Z_1 \cdot Z_3 \cdot Z_5}{(Z_1 \cdot Z_6 + Z_1 \cdot Z_2 + Z_2 \cdot Z_6) \cdot (Z_3 + Z_4 + Z_5) + (Z_1 \cdot Z_3 + Z_3 \cdot Z_6) \cdot (Z_4 + Z_5)} \quad (1)$$

Defining the transfer function of the amplifier, F_A, for the corresponding transfer function of the complete open circuitry holds

$$F_L = F_N \cdot F_A \quad (2)$$

To get both highest accuracy and highest time resolution F_A has to be adjusted to F_N of individual fibres (Pressler 1967; Steinmetz 1979; Duchâteau 1984; Albers 1987). The transfer functions including the phase characteristic of F_L, shown by the dashed lines in Figure 2 (Bode 1945) were calculated for mean effective fibre lengths in the fluid pools. The curves match the corresponding curves given by Nonner (1969). The slope of decay of F_L indicates that by means of F_A stable measuring conditions can be achieved (Steinmetz 1979) and moreover, that at unity cross-over frequency of about 80 kHz the phase reserve, $\alpha = 45°$ (Thomason 1955; Tietze and Schenk 1986),

---

$Z_1 = R_m \| C_m$; $(R_S = 0)$ $\quad$ $Z_4 = R_{CH}$

$Z_2 = R_{HD}$ $\quad$ $Z_5 = R_{CB} \| 1/j\omega C_i$

$Z_3 = 1/j\omega C_B$ $\quad$ $Z_6 = R_{DE}$; $(C_E = 0)$

U_C, U_E: potentials in the corresponding pools. C_i: effective input capacitance of A_1. Note that components being not marked were neglected and that the purpose of switch S is to illustrate the open-loop configuration only.

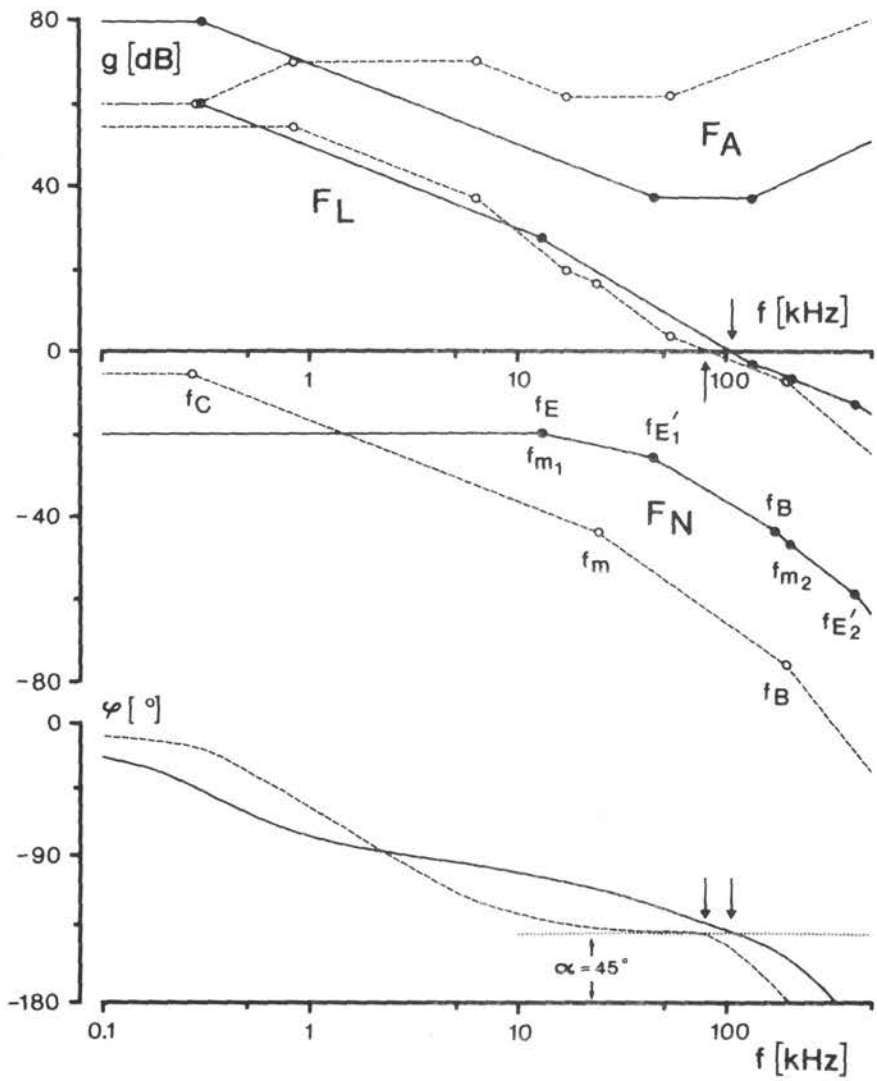

Fig. 2. Bode plot of the original device (dashed curves) and of the extended circuitry (continuous curves). F_N: transfer functions of nerve fibres (diameter: 16 µm and 14 µm, respectively). Corner frequencies of the input stage C, f_C, of pool E, f_E, of pool E′, $f_{E'}$, of the membrane, f_m, and of pool B, f_B, were calculated using mean effective fibre lengths in the fluid pools and standard data for myelinated nerve fibres (Stämpfli and Hille 1976). Note that both $f_{E'}$ and f_m appear twice, the latter if the series resistance is taken into account ($R_S = 600\,k\Omega$). F_A: transfer functions of the belonging amplifiers. F_L: open-loop gain of the respective measuring systems. The corresponding phase shifts, φ, in below. Long arrows indicate unity gain cross-over frequencies and the corresponding phase reserves, α. Dotted line: the $\alpha = 45°$ level.

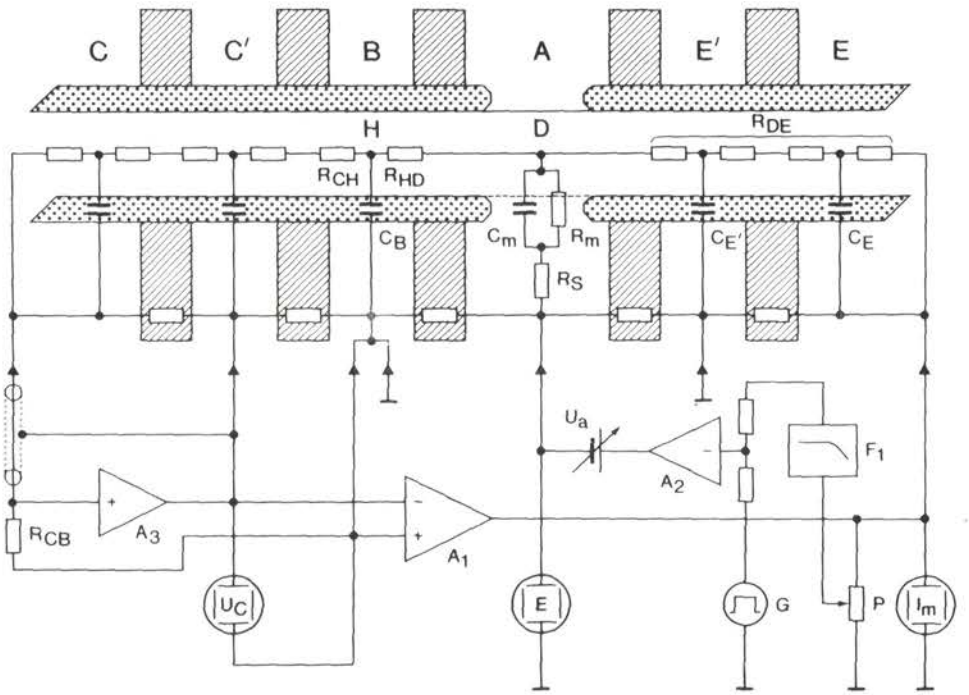

Fig. 3. Schematic diagram of the preparation in the extended potential clamp configuration. The axon is placed across 6 fluid pools C, C', B, A, E', and E of the recording chamber; the node under investigation is in A. The passive axonal components of interest are denoted. Hatched areas: vaseline seals. Filled triangles: Ag/AgCl electrodes. A_1: clamp amplifier. A_2: adder. A_3: low capacitance input probe. G: pulse generator. P: adjustment of amount of positive feedback. F_1: adjustable first order low-pass filter. U_a: adjustment of holding potential, E_H, I_m, E, U_C: oscilloscopes for recording membrane currents, absolute membrane potential and error signals, respectively. $R_{CB} = 6.6$ MΩ. Note that components being not marked were neglected.

is optimized (long arrows). Note however, that these curves are of little practical relevance because of two over-simplifications: 1. The current measuring internode has been assumed to be purely ohmic ($C_E = 0$, thus $Z_6 = R_{DE}$), and 2. The nodal series resistance has been neglected ($R_S = 0$, thus $Z_1 = R_m \| C_m$).

Extended circuitry. The new device (Fig. 3), working basically in the same fashion as the original version exhibits the following extensions: 1. An additional grounded fluid pool, E', between pools A and E (Koppenhöfer and Schumann 1981; Schumann et al. 1983) compensates for the low-pass filter properties of the current measuring impedance, Z_6 ($C_E > 0$). 2. Current proportional positive feedback compensates for the influence of the nodal series resistance ($R_S > 0$). 3. The air gap is replaced by a less noxious vaseline seal (Sommer et al. 1982). 4. A specific broad-banded FET-input stage is introduced (Koppenhöfer and Schumann 1979).

The modified experimental situation is shown schematically in Figure 3. Utilization of the very

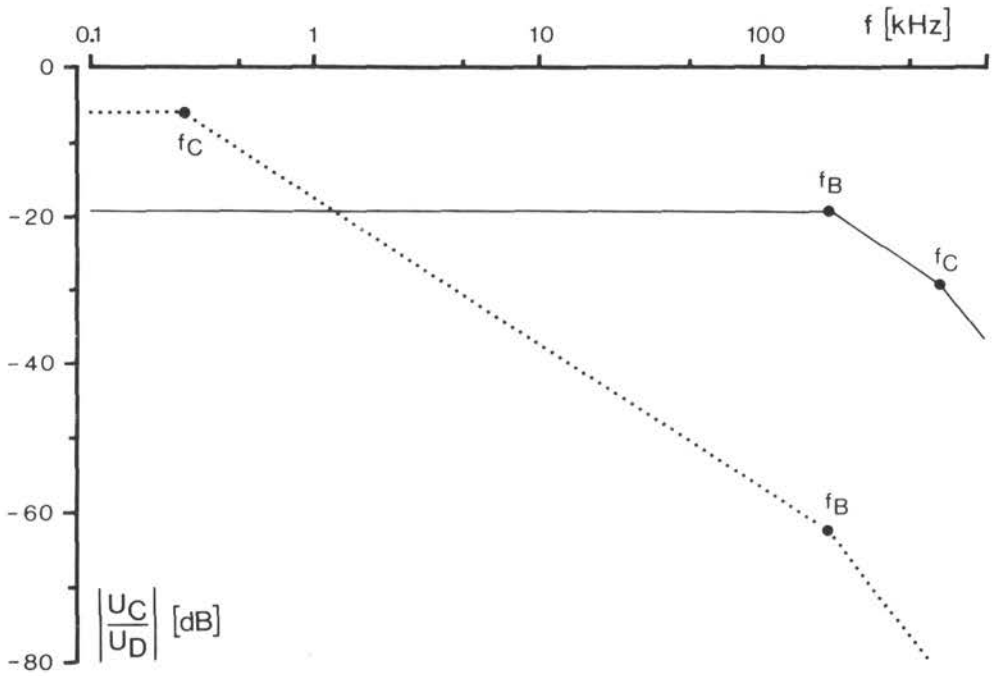

Fig. 4. Transfer functions U_C/U_D of the original configuration (dotted curve) and of the extended circuitry (continuous curve). U_C, U_D: potentials in pool C and at point D, respectively. f_C: effective corner frequencies of the respective input stages. f_B: corner frequency of the low-pass in pool B. Curves were calculated by means of Eq. (3) with $R_{CB} = 100$ MΩ and $C_i = 12.5$ pF (dotted curve) and $R_{CB} = 6.6$ MΩ and $C_i = 0.05$ pF (continuous curve) using mean effective fibre lengths in the fluid pools. Fibre diameter: 16 μm.

low input capacitance of the input probe, A_3, requires surrounding of pool C of the recording chamber from aside and from underneath by an additional pool C′ and by a shield covering thoroughly the C-electrode both driven by A_3. Positive feedback is performed in the conventional manner (Hodgkin et al. 1952) assuming a purely ohmic series resistance, R_S; thus any pulse U is pre-distorted by the output voltage of the clamp amplifier A_1. The desired amount of compensation is set by potentiometer P. Moreover, the time constant of the low-pass filter, F, i.e. the speed of positive feedback, is adjustable as well (not shown).

As mentioned above (Fig. 2) the very low corner frequency of the potential measuring input stage, f_C, is of no practical relevance anymore for the calculation of transfer function of the axon under test, F_N. Therefore, for optimum F_L i.e. $\alpha = 45°$ at comparable unity cross over frequency of about 100 kHz, the clamp amplifier was modified so as to yield the corresponding transfer function, F_A (Fig. 2, continuous curve). It is worth noting that *prima facie* the calculated transfer functions of the original version and of the improved configuration, F_L, do not differ significantly from each other (see, however, p. 428). This is obviously due to inadmissible simplifications of the original version as mentioned above.

In both measuring systems the potential at point D, U_D, (inside the node) is kept near ground

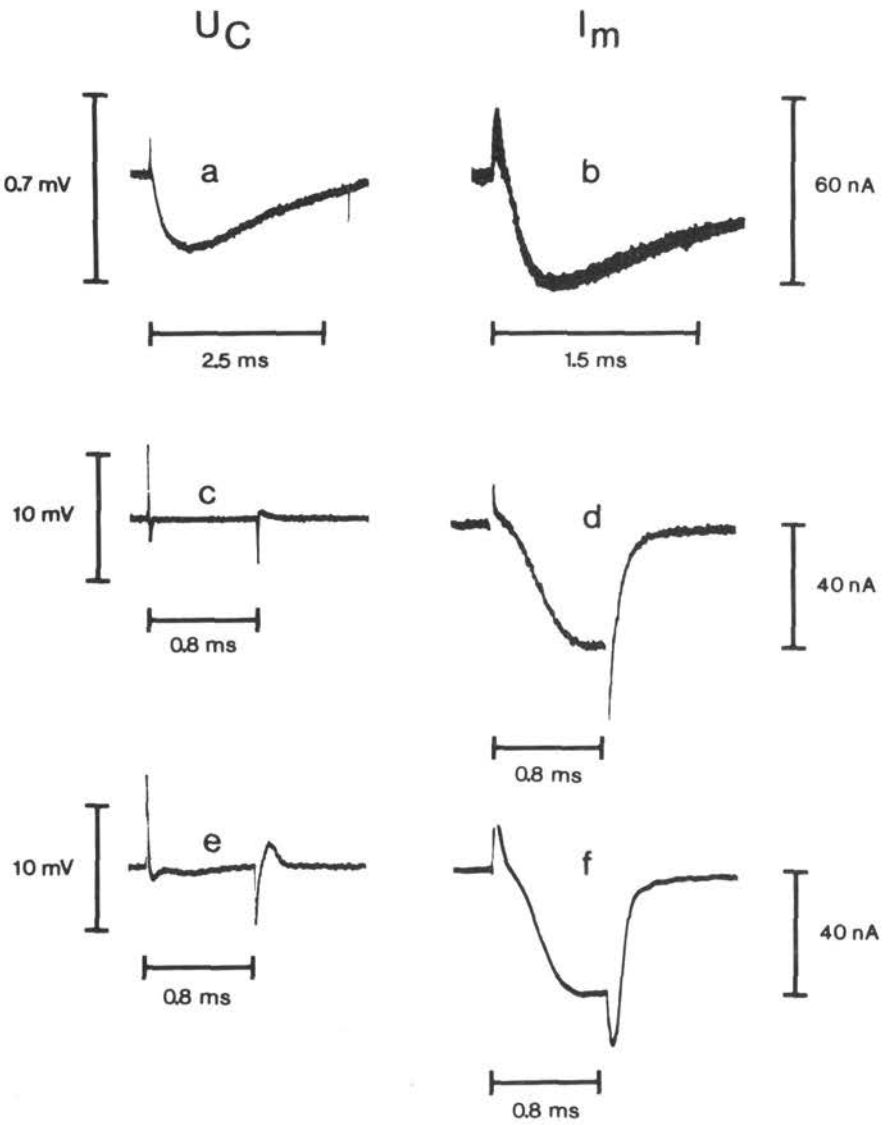

Fig. 5. Membrane currents, I_m, and associated error signals, U_C, elicited by positive test pulses to $E = -10$ mV of 2.9 ms (*a, b*) and 0.8 ms (*c—f*) duration, respectively. *a, b:* original configuration, tuned by means of the capacity surge. Unfiltered signals. Fibre diameter: 18 μm. *c—f:* extended circuitry. Sharp tuning (*c, d*) and flat tuning (*e, f*). Without positive feedback. Signals were filtered by a 4-pole Bessel filter at $f_1 = 100$ kHz (-3 dB). Fibre diameter: 26 μm. For further details see text.

potential by negative feedback. Therefore, the quality of control of the measuring system as limited by any current load of the potential measuring internode between D and pool C, can be tested experimentally by measuring the error signal, U_C. For this the transfer function U_C/U_D has to be calculated:

$$\frac{U_C}{U_D} = \frac{Z_3 \cdot Z_5}{Z_2 \cdot (Z_3 + Z_4 + Z_5) + Z_3 \cdot (Z_4 + Z_5)} \tag{3}$$

The difference between the curves shown in Figure 4 is caused by the huge difference in bandwidth between the respective input stages. The new circuitry exhibits a flat frequency response over the frequency range of interest (Fig. 4, continuous curve) as mentioned above while the corresponding curve obtained with the original setup (dotted curve) is characterized by an input corner frequency of a few hundred Hertz only (Steinmetz 1979).

The error signal with the new circuitry was measured by means of the input stage, A_1, (Fig. 3, oscilloscope "U_C") while with the original setup U_C was tapped non-reactively after the first stage of A_1 (Steinmetz 1979). Figure 5 shows the error signals, U_C, and the associated membrane currents, I_m, obtained with the original version and elicited by relatively long lasting positive test pulses (*a*, *b*) and with the new version (*c*, *d*; *e*, *f*). The latter were elicited by shorter test pulses interrupted at the peak sodium inward current which gave rise to rapidly decaying so-called "sodium tail currents" (see page 428). Note that the differences in amplitudes of error signals between both versions cannot serve as a telling measure for differences in current load of the potential measuring internode, i.e. for quality of control because of the differences in bandwidths between the corresponding transfer functions shown in Figure 4. On the other hand, taking into account the largely frequency independent 20 dB-attenuation of the new version, traces *c*, *d*, *e*, and *f* reflect in fact the underlying changes of U_D at different stages of the tuning procedure (see below). Therefore, at sharp tuning (*c*, *d*) ionic current measurements are now largely free of unwanted current load.

Concerning the original device the frequency response of the amplifier has to be adjusted by means of the criterion "shortest and critically damped capacity currents" (Nonner 1969). In this configuration, however, the capacity currents tell nearly nothing about accuracy and time resolution of ionic current records (Schumann et al. 1983; Wiese and Koppenhöfer 1983). Evidently, a more reliable tuning indicator does not exist.

The new circuitry, however, exhibits a broad-banded access to the main point of interest, D, thus enabling the application of the well-known swept-frequency technique for testing nonlinear networks automatically by a voltage-controlled oscillator of constant amplitude (Schadow 1934): Feeding the command input of the circuitry by a sweep generator of appropriate frequency deviation causes typical error signals (Fig. 6). The tuning procedure starts with increasing DC gain of the amplifier up to maximum, thus reducing the envelope curve as a whole. Selective increase of proportional gain near 100 kHz (see Fig. 2) results eventually in a characteristic hump because of too low phase reserve (Fig. 6*A*) which has to compensated for (*B*) by appropriate differential gain control (Fig. 2, positive branch of F_A). Thereafter, the envelope curve gets its final smooth form (*C*) by shifting the integral gain controller towards higher frequencies (Fig. 2, negative branch of F_A). The remaining frequency dependency of U_C is mainly due to the decrease of loop gain, F_L (see Fig. 2), and the low-pass filter formed by pool B (see Fig. 1). Figure 6 shows that well-defined and sharp tuning is easier to survey by means of a sweep generator than by means of rectangular pulses as can be seen by the corresponding error signals in Figure 5 (*c*, *e*).

Series resistance. Electronic compensation for the influence of the series resistance is characterized 1. by the amount and 2. by the speed of positive feedback. Unfortunately the series resistance cannot be measured directly. Moreover, all non-electric methods for diminishing the influence of R_S known so far (see, e.g., Neumcke and Stämpfli 1982) suffer from considerable imperfections, e.g., they do not enhance the delay in loading the membrane capacitance induced by R_S (Koppenhöfer et al. 1984).

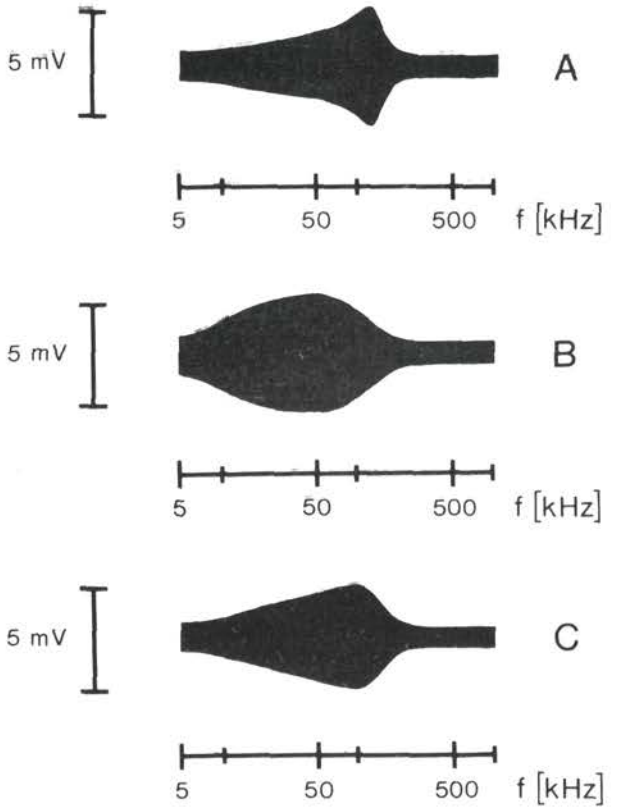

Fig. 6. Frequency response of error signals, U_C, as produced by a voltage-controlled sweep signal generator connected to the command input of the extended circuitry. Sweep width: 5 kHz to 1 MHz. *A, B, C:* At different states of the tuning procedure. *C:* Optimum tuning. Without positive feedback. Fibre diameter: 26 μm. For further details see text.

On the other hand, there are indications for electronic compensation being optimum if the amount of positive feedback, k, is set to shift the minimum of the peak sodium current-voltage curve of the nerve membrane, as measured in normal bathing solution, to zero membrane potential, $E = 0$, (Adelman and Taylor 1964; Grishchenko et al. 1983; Ramón et al. 1975; Wiese and Koppenhöfer 1988). Using the so-called "$E = 0$"-criterion we calculated individual series resistances with $R_S = k \cdot R_{DE}$ (Schumann 1980; Sigworth 1980) and obtained 240 kΩ (median; range 190 to 840 kΩ, $n = 6$). The compensation speed was set as fast as possible throughout. As a rule, 100 kHz at the -3 dB level could be reached.

The characteristic effects of application of the "$E = 0$"-criterion on current-voltage relations are shown in Figure 7. The minimum of the peak sodium current-voltage curve (circles) was shifted to the right by 16 mV (11 to 28 mV, $n = 15$) thus arriving at about $E = 0$ mV(-2 to 2 mV, $n = 15$). Moreover, the intercept of the curve with the potential axis, commonly called "sodium equilibrium

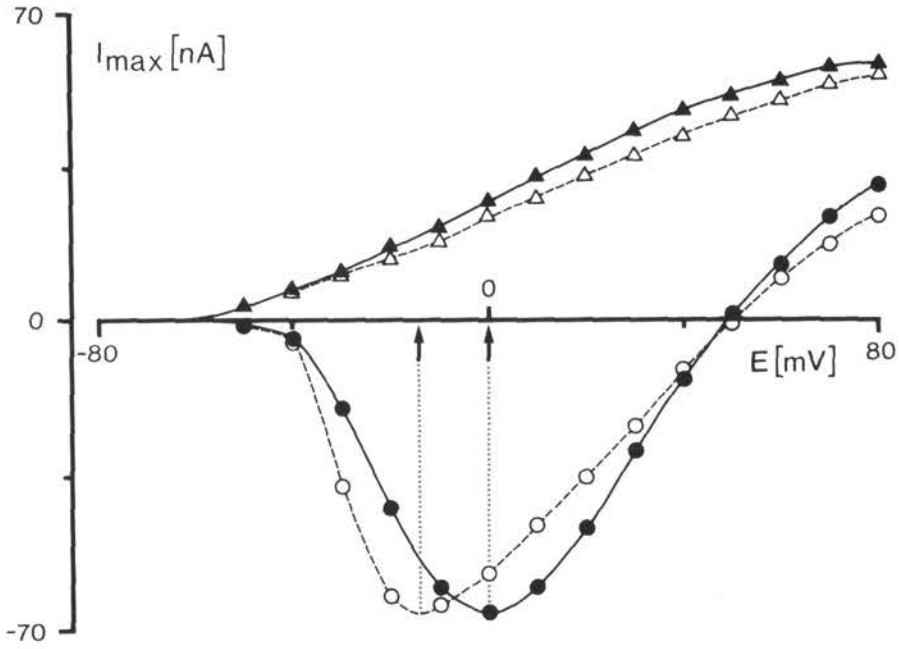

Fig. 7. Current-voltage relations without positive feedback (open symbols) and with optimum compensation for the influence of the series resistance using the "$E = 0$"-criterion (filed symbols). Circles: peak sodium currents. Triangles: maximum potassium currents. The curves were calculated using spline interpolation (Wiese and Koppenhöfer 1988). Arrows indicate position of curve minima on the potential axis. $R_S = 230$ kΩ.

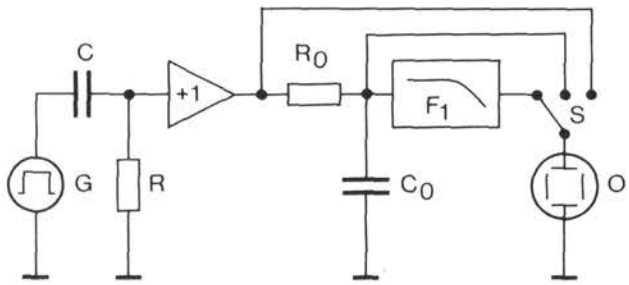

Fig. 8. Setup for testing the distortion of exponentially decaying test pulses by two low pass filters in series. G, C, R: device delivering exponentially decaying test pulses of $\tau = 10$ μs *via* buffer (+1). R_0, C_0: low pass filter ($f_0 = 100$ kHz) represeting the potential clamp system *per se*. F_1: switchable 4-pole Bessel filter ($f_1 = 80$, 40, 20 kHz, respectively) as used in potential clamp experiments (not shown in Fig. 3); S: input selector of oscilloscope O for recording test pulses, pulses distorted by the replica of the potential clamp system, and pulses filtered additionally by the external filter, F_1.

potential", E_{Na}, was slightly shifted to the left by -1 mV (-3 to 1 mV, $n = 15$). This is due to the fact that positive feedback compensates for any current load of R_S (Koppenhöfer et al. 1984). In addition, the maximum potassium current-voltage relation (triangles) was clearly shifted to the left as has been described for the squid axon at zero series resistance (Adelman and Taylor 1964), and saturated at strong positive test pulses.

Noise reduction. Inappropriate signal to noise ratios of membrane current records are commonly improved by low-pass filters. As a matter of fact, however, the so-called "over-filtering" by a too low corner frequency of the filter used as compared to the fastest components of the signals to be evaluated reduces the significance of kinetics and even of peak values of current signals. Obviously so-called "tail current measurements" on sodium activation are most liable to get distorted this way. Therefore, we tested the effects of various corner frequencies on single pulses decaying with a time constant close to those found in sodium tail current experiments (see page 428) by means of the test circuit shown in Figure 8. The filter property of the clamp device *per se* was simulated by a first order low-pass filter ($C_2 \cdot R_2$) in series to the switchable filter F_1 under test. The effect of finite bandwidth of the potential clamp circuit (Fig. 9*A*, *b*) on the time course of pulses decaying unconstrainedly with $\tau = 10$ μs (*a*) proved negligibly small. The corresponding instantaneous value (Fig. 9*B*, *b*, filled symbols), however, increased by about 13 % as compared to the initial value of curve *"a"*; this has to be attributed to the inevitable delay time of the clamp device (Fig. 9*A*, t_h). Any additional filtering (*c*, *d*, *e*) coarsed the effect resulting in additional changes of the slope of decay at strong over-filtering (*e*).

Therefore, to ensure decent signal to noise ratios in sodium tail current measurements we had to begin with the technique of signal-averaging introduced, to our knowledge in electrophysiology by Dawson (1951): Four to 32 current records elicited by identical test pulses at a repetition frequency of about 1 Hz and of a so-called jitter of less than 100 ns as referred to the preceding trigger pulse were condensed at a sampling frequency of 250 kHz and at a resolution of 12 Bit by adding the samples and dividing their sum by the number of samples. Although this procedure of noise reduction requires current signals of considerable stability it represents the farthest limit to which measurements of fast components of membrane currents can be pushed at the present time.

For comparison, sodium currents elicited by strong positive test pulses were filtered at different corner frequencies, f_1, and compared to corresponding records which were signal-averaged instead of being filtered. The current kinetics as tested at 15 °C proved sufficiently slow to get filtered at $f_1 = 80$ kHz without significant perturbance. Therefore, no signal-averaging was necessary for ordinary peak sodium current voltage relations and for evaluation of the underlying current kinetics.

Results

Kinetics of sodium currents. Following the HHF-formalism the kinetics of sodium currents in Ranvier nodes are described by time constants of activation and inactivation, τ_m and τ_h, respectively,

$$[1 - \exp(-t/\tau_m)]^2 \cdot \exp(-t/\tau_h) \quad (4)$$

(Frankenhaeuser 1960). Moreover, the potential dependences of the time constants follow monotonous curves decaying with increasing positive test pulse amplitudes above threshold. Therefore, the time to peak sodium current, t_{peak},

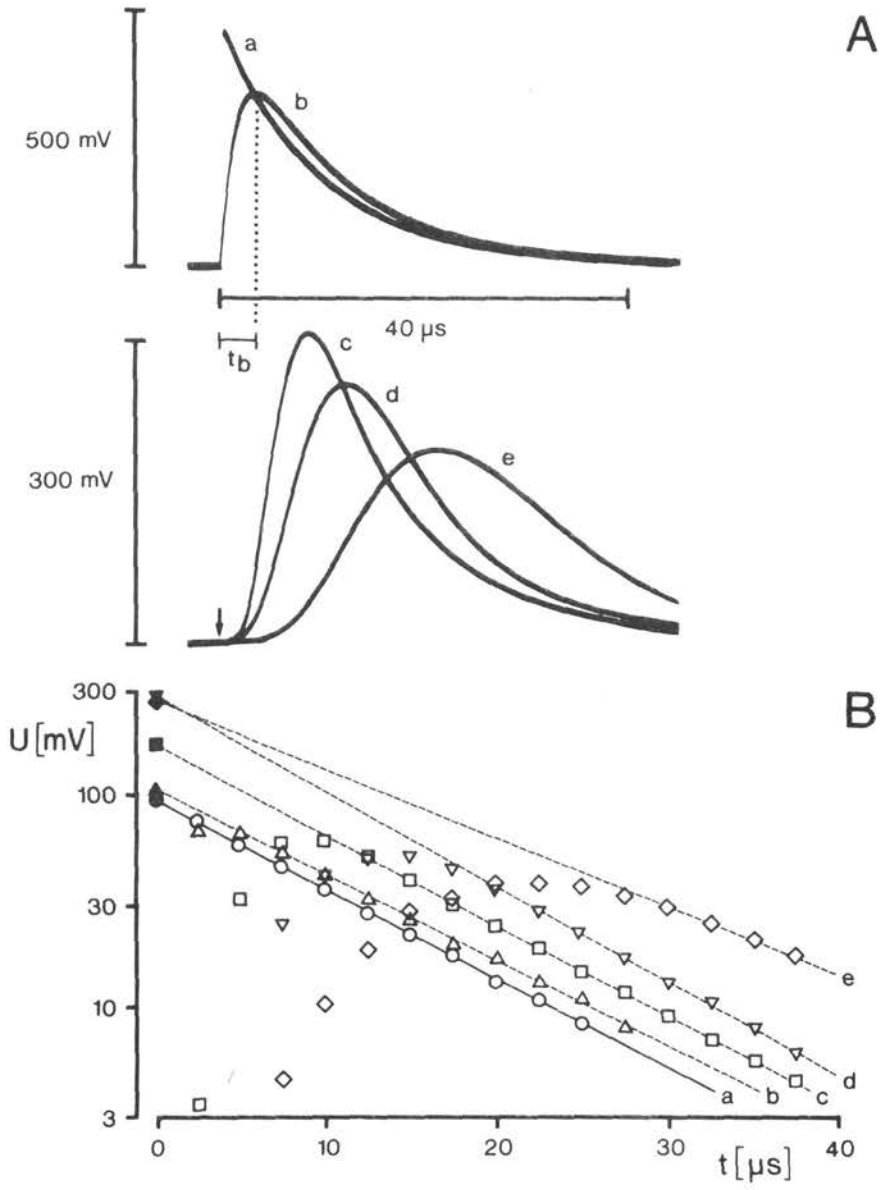

Fig. 9. Distortion of exponentially decaying pulses generated by the test circuit shown in Figure 8. *A:* time course of test pulse (*a*) and of the signal distorted by the replica of the potential clamp system *per se* (*b*). Note delay time, t_b, of the measuring system. *c, d, e:* additional distortion by the switchable filter, F_t, at corner frequencies of 80, 40 and 20 kHz, respectively. The arrow indicates the start of test pulse (*a*). *B:* semilog plot of traces shown in *A* (open symbols) as related to the start of test pulse (*a*). Linear extrapolation of the decay yielded corresponding instantaneous values for $t = 0$ (filled symbols).

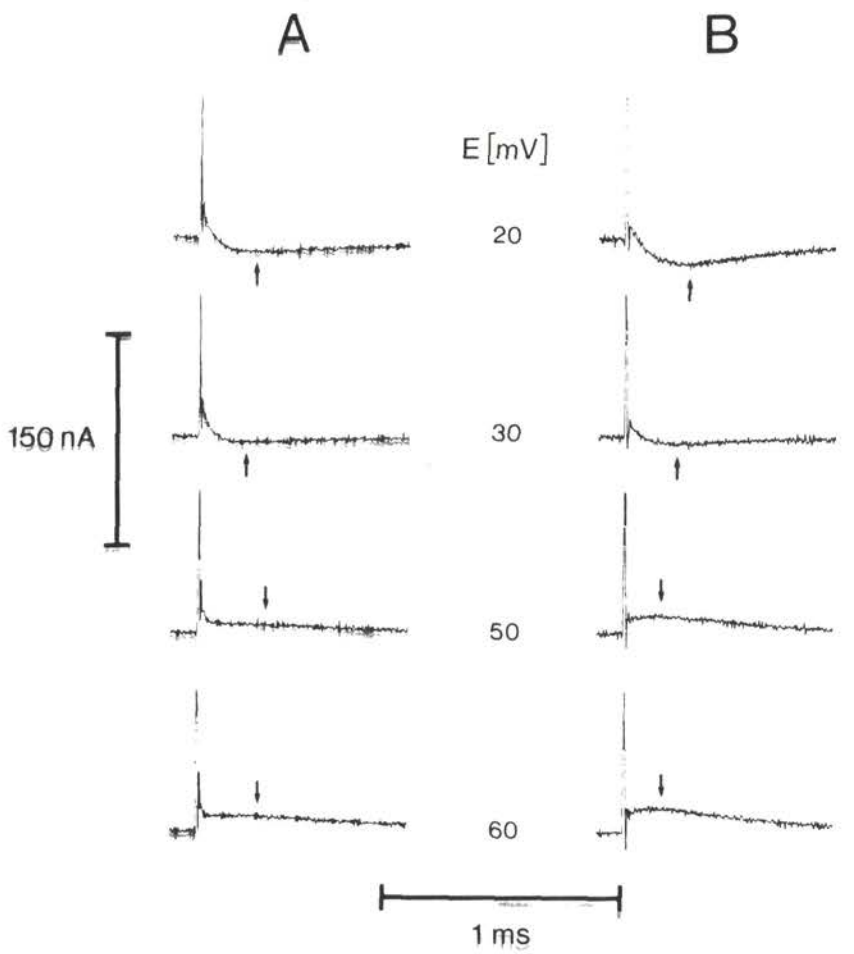

Fig. 10. Current records elicited by positive steps to potentials around the sodium equilibrium potential. Peak sodium currents are indicated by arrows. *A:* without positive feedback. *B:* under positive feedback. Records were filtered (f_l = 80 kHz). The ends of the trace are cut. R_S = 840 kΩ. Note that for shortest settling time the system was slightly hypercritically tuned as indicated by a short undershoot in the decay of the capacity current.

should change monotonously as well. When potential steps close to the sodium equilibrium potential were applied it became evident that this was the case only provided the influence of the series resistance was properly compensated for (Fig. 10*B*). Without positive feedback (Fig. 10*A*), however, as soon as the current changed its direction (E = 50 mV) a sudden increase of t_{peak} became detectable, although clearly less pronounced than observed in corresponding

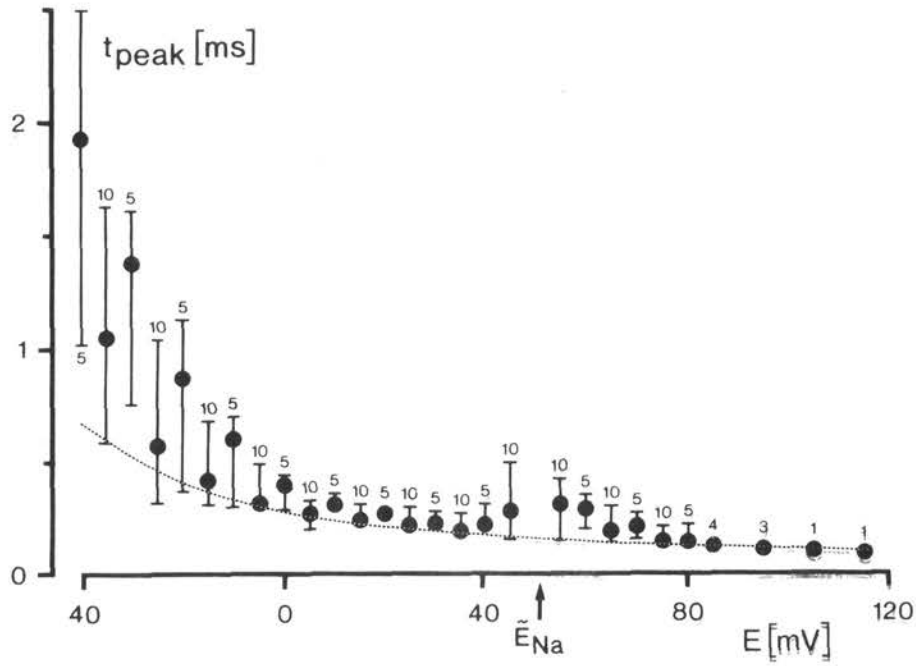

Fig. 11. Time to peak sodium currents, t_{peak}, as function of membrane potential, E. Symbols, bars and figures denote medians, ranges and numbers of measured values, respectively, obtained from 8 fibres. Note that the potential axis was normalized to the median of the sodium equilibrium potential $\tilde{E}_{Na} = 49$ mV under optimum positive feedback. Dotted line: $t_{peak} - E$ curve as calculated from standard data (Frankenhaeuser 1960) by means of the expression: $t_{peak} = \bar{\tau}_m \cdot \ln(2 \cdot \bar{\tau}_h/\bar{\tau}_m + 1)$ (Tuszynski 1989).

experiments performed with the original circuitry (see Koppenhöfer and Bohuslavizki 1988, Fig. 1).

Aimed at a more detailed analysis positive pulses were applied up to $E = 115$ mV under positive feedback and t_{peak} was plotted *versus* membrane potential. Individual t_{peak} -E curves were lumped together by correcting their potential axis for the deviation of their respective sodium equilibrium potential, E_{Na}, from the median of E_{Na}, $\tilde{E}_{Na}$. The plot of all data applies for $\tilde{E}_{Na}$ (Fig. 11). As expected from the records shown in Figure 10*B* the decay of the t_{peak} is in fact largely monotonous. The small hump near $\tilde{E}_{Na}$ is of little significance as compared to the corresponding data from experiments performed with the original circuitry (see Koppenhöfer and Bohuslavizki 1988, Fig. 2).

Sodium permeability. According to the HHF-formalism for the sodium per-

meability of Ranvier nodes, P_{Na}, holds

$$P_{Na} = \bar{P}_{Na} \cdot m^2 \cdot h, \tag{5}$$

where both the activation and the inactivation variable, m and h, are unique functions of membrane potential, E. Therefore, the definition of P_{Na} should account for the so-called "sodium rectification" (see, e.g., Khodorov 1974) in a sense that the peak P_{Na} -E curve should be S-shaped. For this purpose the constant field equation has been introduced as a suitable definition of P_{Na} in Ranvier nodes (Dodge and Frankenhaeuser 1959):

$$P_{Na} = I_{Na} \cdot \frac{R \cdot T}{F^2 \cdot E \cdot [Na]_o} \cdot \frac{\exp(EF/RT) - 1}{\exp[(E - E_{Na}) \cdot F/RT] - 1} \tag{6}$$

($[Na]_o$: external sodium concentration; R, T and F have their usual meaning).

We repeated the principal experiments of Dodge and Frankenhaeuser (1959) in the same fashion as described in our foregoing paper (Koppenhöfer and Bohuslavizki 1988): Test pulses up to $E = 110$ mV were applied and peak P_{Na} was calculated from peak sodium currents by Eq. (6). A sigmoid function corresponding to the commonly adopted equation describing the potential dependence of the inactivation variable h (Frankenhaeuser 1959)

$$\text{peak } P_{Na} = P_{Na\,max} \cdot \left[\frac{1}{1 + \exp[(E_h - E)/k_h]}\right]^2 \tag{7}$$

was fitted to the data (Benoit and Dubois 1987). Bearing in mind that in Ranvier nodes potential values between resting potential and sodium equilibrium potential only are of functional relevance to the living animal it was obvious to use data derived at $E < E_{Na}$ only. The fit carried out in this way yielded numerical values for the potential at rohich peak P_{Na} is half of $P_{Na\,max}$, E_h, the steepness factor, k_h, and in particular, for the maximum peak permeability, $P_{Na\,max}$. Normalizing peak P_{Na} to $P_{Na\,max}$ yielded curves which were lumped together in the same fashion as in the experiments concerning the potential dependence of t_{peak}: i.e., the potential axis of individual experiments was corrected to the median of the respective sodium equilibrium potentials measured ($\tilde{E}_{Na} = 49$ mV; range 34 to 60 mV, $n = 15$). Subsequently Eq. (7) was fitted to the medians of the normalized P_{Na} values at $E < \tilde{E}_{Na}$ (Fig. 12, dashed line and filled symbols, respectively). For comparison, measuring points which were ignored (open symbols) are given as well. No doubt, in spite of the considerable scatter the calculated curve reasonable well fits the medians in the potential range tested: nonlinear regression coefficient $r_{nl} = 0.9957$ (Sachs 1984). The open symbols (representing measurements beyond the sodium equilibrium potential), however, have evidently little to do with the sigmoid function postulated by the HHF-formalism. Moreover, upon incorporating these data nothing else was

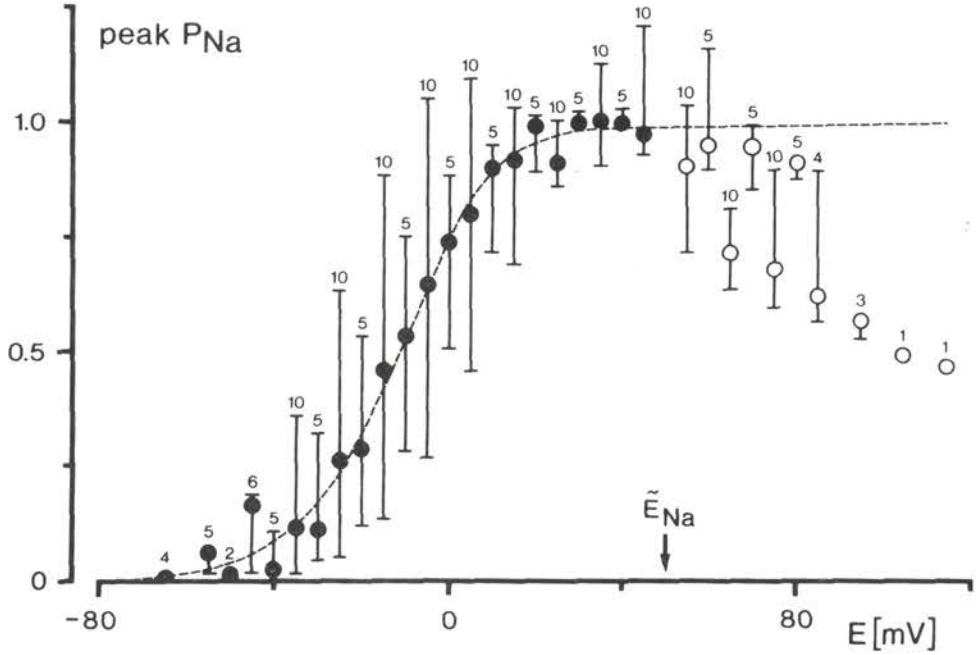

Fig. 12. Normalized peak sodium permeability, peak P_{Na}, as function of membrane potential, E. Symbols, bars and figures denote medians, ranges and numbers of measured values, respectively, obtained from 8 fibres. Equation (6) was fitted (dashed line) to the data derived at $E < E_{Na}$ (filled symbols). Note that the potential axis was normalized to the median of the sodium equilibrium potential $\tilde{E}_{Na} = 49$ mV under optimum positive feedback. Data from $E > E_{Na}$ (open symbols) are shown for comparison. For further details see text.

obtained as systematic deviations from the calculated curve near E_{Na} indicating that data measured outside of the biological operation range of the membrane are controlled by additional mechanisms which are of little relevance to the nerve function in the living animal.

For comparison, we repeated the treatment of peak I_{Na} described above using a potential dependent sodium conductance, g_{Na}, as introduced by Hodgkin and Huxley (1952) for the unmyelinated axon

$$\text{peak } g_{Na} = \frac{\text{peak } I_{Na}}{E - E_{Na}} \tag{8}$$

instead of P_{Na} as defined by Eq. (6). Although we used data from the potential range of biological relevance only the fit was less satisfactory ($r_{nl} = 0.9893$) than the corresponding peak P_{Na} curve shown in Figure 12.

Assuming both the ratio of the time constants of sodium currents, τ_m/τ_h,

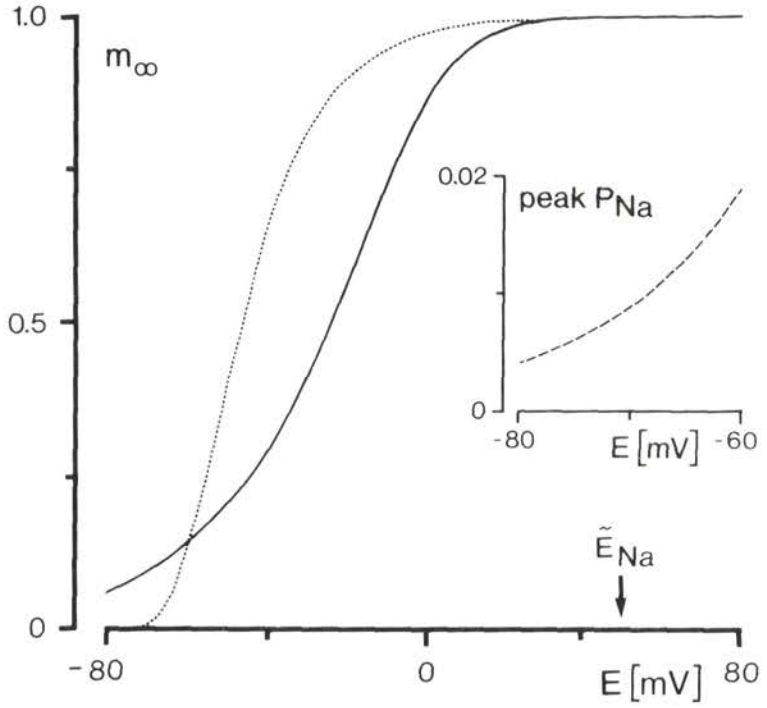

Fig. 13. Activation curves. Continuous line: calculated from the dashed line in Figure 12. Dotted line: activation curve from Frankenhaeuser (1960), redrawn. Inset: peak P_{Na} (dashed line) of Figure 12 near $E_R = -80$ mV, drawn to a larger scale.

and the power of the activation term to be largely potential independent (Frankenhaeuser 1960) the square root of the peak P_{Na}-curve represents the potential dependence of the activation term, m, (Fig. 13, continuous curve). Extrapolation to $E_R = -80$ mV yielded $m_{ER} = 0.065$ whereas m at rest is expected to be almost zero (Frankenhaeuser and Huxley 1964: m_{ER}: 0.0005) as indicated by the dotted curve in Fig. 13 (Frankenhaeuser 1960). However, both curves differ mainly in potential at which $m_\infty = 0.5$, ($E_h = -25$ mV and -38 mV, respectively) and in steepness ($k_h = 19$ mV and 13 mV, respectively) as well.

Fig. 14. Membrane currents elicited with test pulses to $E_1 = 0$ mV interrupted close to peak sodium current by repolarization to $E_2 = -80$ mV ($= E_R$). *A*: traces show averaged signals of 16 records each. *a, c*: without positive feedback; *b, d*: under optimum positive feedback; *a, b*: narrow-banded, conventional current measuring internode; *c, d*: broad-banded current measuring internode. Arrows indicate end of current during E_1, I_{Na1}. Dotted line: zero current. *B*: semilogarithmic plot

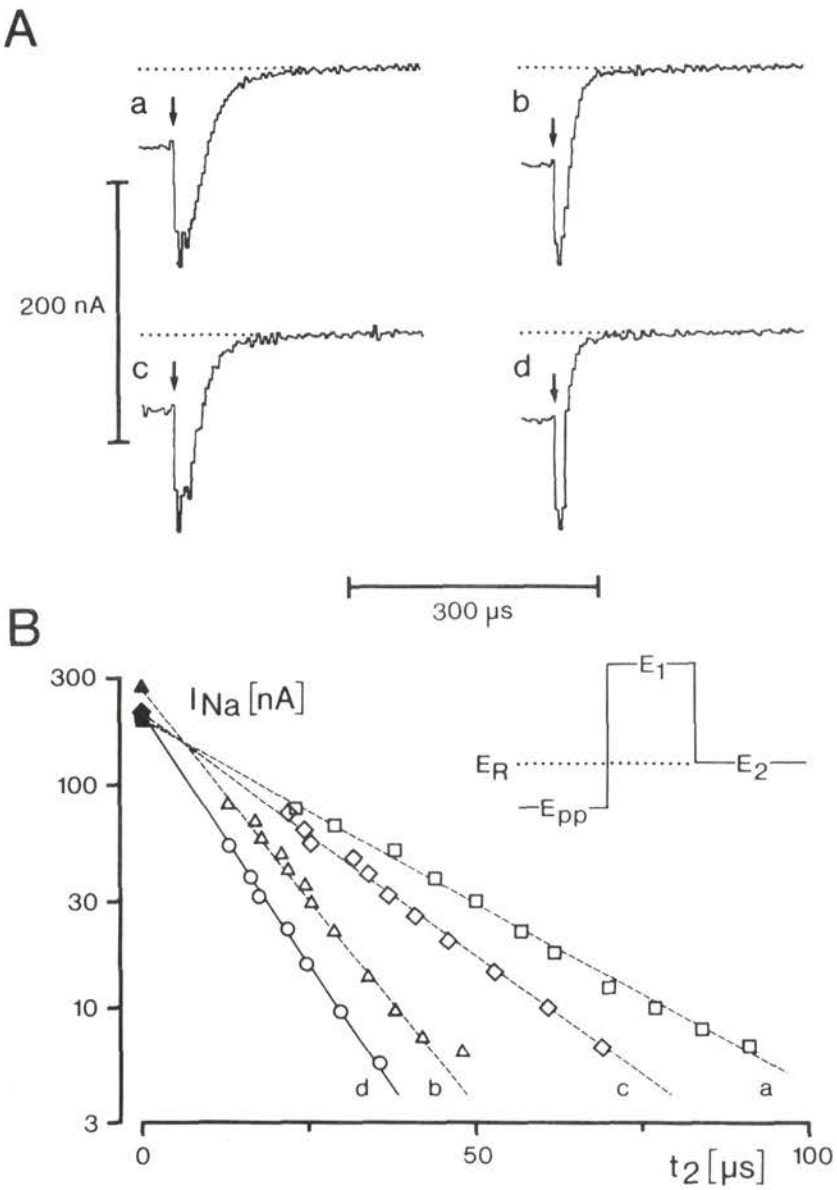

of sodium tail currents during E_2 and pulse program used (inset), the latter not drawn to scale. Linear extrapolation of currents (open symbols) by least square fit regression to the beginning of repolarization (*A*: arrows, *B*: $t_2 = 0$) yielded instantaneous sodium currents, I_{Na2} (filled symbols). $R_S = 260$ kΩ. For further details see text.

If the constant field concept were an appropriate definition of the sodium permeability in the biological operation range of the nodal membrane P_{Na} should change at potential steps below E_{Na} with finite speed only. This was tested under different measuring conditions in the so-called "sodium tail current"-experiments. Positive test steps to $E_1 = 0$ mV were terminated by repolarizing the membrane around peak sodium inward current, I_{Na1}, (Fig. 14*A*, arrows) to $E_2 = E_R = -80$ mV (see inset). The sudden increase in driving force for sodium ions at the beginning of E_2 caused a sudden increase of sodium current which after the capacitive surge decayed with different slope depending clearly on the measuring conditions chosen. Note that introduction of both a broad-banded current measuring internode (a → c) and optimum positive feedback (b → d) enhance the clearly exponential decay of "tail current" (*B*). Moreover, linear extrapolation of the "tail currents" in B to the beginning of repolarization ($t_2 = 0$) yielded instantaneous currents, I_{Na2}, (Fig. 14*B*, filled symbols) which obviously depend on the measuring conditions chosen. From I_{Na1} and I_{Na2} we calculated the corresponding permeabilities P_{Na1} and P_{Na2} by Eq. (6) using values of E_{Na} as measured on the respective axon. Surprisingly, under no measuring conditions tested was the ratio P_{Na2}/P_{Na1} unity as it should be the case if equation 6 properly accounted for the discontinuity of sodium currents: Under optimum measuring conditions (Fig. 14, *d*) the median was 0.84 (range 0.30 to 10.61, $n = 14$) indicating a left-steep distribution of the data (Sachs 1984).

As mentioned above sodium tail currents decay faster under optimum measuring conditions (Fig. 14, *d*) as compared to conventional measuring conditions (a). Thus, assuming the power of the *m*-term being two (see page 424) the time constant of activation, τ_m, amounts to 25.4 μs (range 14.8 to 45.0 μs, $n = 14$) at $E = 0$ mV and 10 °C rather than about 170 μs as referred to the so-called standard data of the HHF-formalism (Frankenhaeuser 1960; Frankenhaeuser and Moore 1963).

Discussion

1. Measuring conditions. The accuracy of measuring systems for recording membrane currents in Ranvier nodes used so far bases mainly on two simplifications: 1. The current measuring internode is largery ohmic, and 2. the nodal membrane is the only impedance worth mentioning between point D inside the node and pool A of the recording chamber. In addition, the commonly used measuring system after Nonner (1969) implies that 1. dessication of the internode in the air gap does not inflict changes of the measuring conditions, and 2. any unwanted current load of the node under investigation during membrane current measurements is prevented. Although for decent measuring conditions

these postulates are mandatory each of them got recently falsified (for references see section "Introduction"). Therefore, following well-known principles of non-linear servo theory methodical improvements were inserted (see page 414) which minimized the errors in measurement introduced by over-simplifications and technical imperfections mentioned near to the limit to which they can be pushed at present with a one-loop measuring system. This procedure offers the chance for better grounded conclusions drawn from more reliable experimental results in Ranvier nodes than previously because "at best the criterion must be in agreement within the limits of accuracy of the measuring instruments employed" (Kuhn 1961). Moreover, the new circuitry allows to control the main interfering variables which take share in sources of the so-called biological scatter of data. Therefore, e.g. investigations of drug effects can now be shortened and the number of animals to be sacrificed can be considerably reduced.

2. *Sodium permeability*. Evidently, the kinetics of small sodium currents near E_{Na} are particularly sensitive to technical imperfections known from conventional setups. This should be considered when introducing drug-induced transformation of sodium channels (Benoit and Dubois 1987).

Our experiments designed to study the potential dependence of peak sodium currents showed that the constant field formalism nicely fits the data in the potential range of biological relevance ($E < E_{Na}$). At more positive potentials, however, additional mechanisms make the data distorted out of all resemblance to a sigmoid function. Therefore, we doubt that data derived on both sides of E_{Na} should be pooled when estimating the constant field formalism for peak sodium permeability of relevance to the living animal.

In our opinion, the formal validity of equation (6) for data measured below E_{Na} does not necessarily imply a *de facto* linear potential gradient along the sodium channel. This view gets support from the generally accepted hypothesis both of negative fixed charges on either side of excitable membranes (see e.g. Chandler et al. 1965; Frankenhaeuser and Hodgkin 1957; Mozhayeva and Naumov 1970; Vogel 1974) and of membrane dipoles (see e.g. Armstrong and Bezanilla 1973; Keynes and Rojas 1973; Meves et al. 1988).

It seems worth noting that when pooling the data from Figure 12 without normalizing the potential axis to $\tilde{E}_{Na}$ the scatter of peak P_{Na}-values was considerably diminished, thus the effective gradient of sodium concentration in individual nodes varies more clearly than expected. The deviation of the underlying activation curve from the corresponding standard curve in Figure 13, however, is of low significance as the power of the activation term has been assumed in accordance with the standard data instead of having been measured under proper measuring conditions.

The results concerning instantaneous sodium currents ask for some com-

ments: In fact, under optimum measuring conditions the median P_{Na2}/P_{Na1} is reasonably close to unity as expected from the validity of the constant field formalism in the respective potential range. The clearly left-steep distribution of P_{Na2}/P_{Na1}, however, suggests that in accordance with the model experiments shown in Figure 9, in certain instances the corner frequency of the measuring system used in our experiments was considerably smaller than assumed, i.e. $f_0 < 100$ kHz.

3. Potassium currents. After the current working model for the differentiation of the nodal membrane (see, e.g., Waxman 1985) potassium channels are clustered paranodally, in part underneath the myelin loops bordering the nodal gap while sodium channels are mainly located in the central area of the nodal membrane. Taking into account the central outbulging of the nodal membrane seen in thick nerve fibres (M. Rydmark, personal communication) the effective series resistance working on potassium channels should be systematically higher than the series resistance working on sodium channels. Therefore, trusting in any criterion for optimum compensation as derived from sodium current measurements, the effect of the series resistance of potassium channels should be systematically undercompensated. This might be the reason for the effect of positive feedback on the potassium current- voltage relation (see Fig. 7) being smaller than expected (see Ramón et al. 1975).

4. Still finite reliability of data. The reliability of potential clamp data in Ranvier nodes is still determined primarily by 1. the absence of a direct criterion for optimum positive feedback in Ranvier nodes (see, however, Salzberg and Bezanilla 1983), 2. the assumption of a simple ohmic behaviour of the nodal gap structures which has been made because of technical practicability rather than because of electronmicroscopical evidence (see, e.g., Berthold and Rydmark 1983 b), and 3. by the assumption of a largely homogeneous internodal impedance. Apart from the Schmidt-Lanterman incisures (for references, see Landon and Hall 1976) this might be not very far from being correct (R.-G. Sommer, personal communication).

Moreover, inherent disadvantages of the system in our experiments used include: 1. Relatively low maximum gain between pool C and E of not more than 80 dB, and 2. indirect control of the tuning procedure by means of the error signal between pool C and B instead of direct monitoring of the frequency response of the membrane potential equivalent in pool A. Limitations of this kind render difficult both to prevent current load of the potential measuring internode and to achieve sufficiently high cross-over frequencies. It will be demonstrated in a forthcoming paper that starting from a two-loop measuring system (Kneip 1987) such shortcomings can be overcome; thus solid measure-

ments even of the power of the *m*-term (Neumcke et al. 1976), of capacity currents and, in particular, of asymmetrical currents come in reach.

Acknowledgments. We thank Dipl. Phys. A. Kneip for installing the data processing-equipment and Dr. H. Wiese for valuable comments.

References

Adelman W. J. Jr., Taylor R. E. (1964): Effects of replacement of external sodium chloride with sucrose on membrane currents of the squid giant axon. Biophys. J. **4,** 451—463

Albers M. (1987): Ionenstrommessungen an myelinisierten Nervenfasern unter optimalen Meßbedingungen — Das Verfahren nach Nonner. Thesis, University of Kiel

Armstrong C. M., Bezanilla F. (1973): Currents related to the movement of the gating particles of the sodium channel. Nature (London) **242,** 459—461

Benoit E., Dubois J.-M. (1987): Properties of maintained sodium current induced by a toxin from *Androctonus* scorpion in frog node of Ranvier. J. Physiol. (London) **383,** 93—114

Berthold C.-H., Rydmark M. (1983a): VI. Anatomy of the paranode-node-paranode region in the cat. Experientia **39,** 954—976

Berthold C.-H., Rydmark M. (1983b): Electron microscopic serial section analysis of nodes of Ranvier in lumbosacral spinal roots of the cat: Ultrastructural organization of nodal compartments in fibres of different sizes. J. Neurocytol. **12,** 475—505

Bethge E. W., Bohuslavizki K. H., Koppenhöfer E. (1989): An inert hydrogen ion buffer for sodium current measurements in Ranvier nodes. Gen. Physiol. Biophys. **8,** 505—508

Bode H. W. (1945): Network Analysis and Feedback Amplifier Design. v. Nostrand Company, New York

Chandler W. K., Hodgkin A. L., Meves H. (1965): The effect of changing the internal solution on sodium inactivation and related phenomena in giant axons. J. Physiol. (London) **180,** 821—836

Clarke E., Bearn J. G. (1972): The spiral nerve bands of *Fontana*. Brain **95,** 1—20

Dawson G. D. (1951): A summation technique for detecting small signals in a large irregular background. J. Physiol. (London) **115,** 2P

Dodge F. A., Frankenhaeuser B. (1958): Membrane currents in isolated frog nerve fibre under voltage clamp conditions. J. Physiol. (London) **143,** 76—90

Dodge F. A., Frankenhaeuser B. (1959): Sodium currents in the myelinated nerve fibre of *Xenopus laevis* investigated with the voltage clamp technique. J. Physiol. (London) **148,** 188—200

Duchâteau R. (1984): Ein Verfahren zur Messung von Ionenströmen an myelinisierten Nervenfasern — Minimierung systematischer Meßfehler. Thesis, University of Kiel

Frankenhaeuser B. (1959): Steady state inactivation of sodium permeability in myelinated nerve fibres of *Xenopus leavis*. J. Physiol. (London) **148,** 671—676

Frankenhaeuser B. (1960): Quantitative description of sodium currents in myelinated nerve fibres of *Xenopus laevis*. J. Physiol. (London) **151,** 491—501

Frankenhaeuser B., Hodgkin A. L. (1957): The action of calcium on the electrical properties of squid axons. J. Physiol. (London) **137,** 218—244

Frankenhaeuser B., Huxley A. F. (1964): The action potential in the myelinated nerve fibre of *Xenopus laevis* as computed on the basis of voltage clamp data. J. Physiol. (London) **171,** 302—315

Frankenhaeuser B., Moore L. E. (1963): The effect of temperature on the sodium and potassium permeability changes in myelinated nerve fibres of *Xenopus laevis*. J. Physiol. (London) **169,** 431—437

Grishchenko J. J., Naumov A. P., Zubov A. N. (1983): Gating and selectivity of aconitine-modified sodium channels in neuroblastoma cells. Neuroscience **9,** 549—554

Hodgkin A. L., Huxley A. F. (1952): A quantitative description of membrane current and its application to conduction and excitation in nerve. J. Physiol. (London) **117,** 500—544

Hodgkin A. L., Huxley A. F., Katz B. (1952): Measurement of current-voltage relations in the membrane of the giant axon of *Loligo*. J. Physiol. (London) **116,** 424—448

Keynes R. D., Rojas E. (1973): Characteristics of the sodium gating current in squid giant axons. J. Physiol. (London) **233,** 28P

Khodorov B. I. (1974): The Problem of Excitability. Plenum Press, New York

Kneip A. (1987): Ionenstrommessungen an myelinisierten Nervenfasern unter optimierten Meßbedingungen – Das Verfahren nach Frankenhaeuser. Thesis, University of Kiel

Koppenhöfer E., Bohuslavizki K. H. (1988): Inconsistent sodium current records derived on Ranvier nodes with a commercially available potential clamp device according to Nonner. Gen. Physiol. Biophys. **7,** 557—567

Koppenhöfer E., Schumann H. (1979): Fast potential clamp measurements on the node of Ranvier. Pflügers Arch. **379,** R42

Koppenhöfer E., Schumann H. (1981): A method for increasing the frequency response of voltage clamped myelinated nerve fibres. Pflügers Arch. **390,** 288—289

Koppenhöfer E., Wiese H., Schumann H., Wittig J. (1984): Experimente zum Einfluß des Serienwiderstandes auf die Potentialabhängigkeit der Natriumspitzenströme des Ranvierschen Schnürrings. Funkt. Biol. Med. **3,** 61—64

Koppenhöfer E., Sommer R.-G., Froese U. (1987): Effects of benzocaine and its isomers on sodium permeability and steady state inactivation in the myelinated nerve, obtained by an improved dissection technique. Gen. Physiol. Biophys. **6,** 209—222

Kuhn T. S. (1961): The function of measurement in the modern physical science. Isis **52,** 161—193

Landon D. N., Hall S. (1976): The myelinated nerve fibre. In: The Peripheral Nerve (Ed. D. N. Landon), pp. 1—105, Chapman and Hall, London

Meves H., Rubly N., Stämpfli R. (1988): The action of arginine-specific reagents on ionic and gating currents in frog myelinated nerve. Biochim. Biophys. Acta **943,** 1—12

Mozhayeva G. N., Naumov A. P. (1970): Effect of surface charge on the steady-state potassium conductance of nodal membrane. Nature (London) **228,** 164—165

Neumcke B., Nonner W., Stämpfli R. (1976): Asymmetrical displacement current and its relation with the activation of sodium current in the membrane of frog myelinated nerve. Pflügers Arch. **363,** 193—203

Neumcke B., Stämpfli R. (1982): Sodium currents and sodium current fluctuations in rat myelinated nerve fibres. J. Physiol. (London) **329,** 163—184

Nonner W. (1969): A new voltage clamp method for Ranvier nodes. Pflügers Arch. **309,** 176—192

Pressler G. (1967): Regelungstechnik. Bibliographisches Institut, Mannheim

Ramón F., Anderson N., Joyner W., Moore J. W. (1975): Axon voltage clamp simulations. IV. A multicellular preparation. Biophys. J. **15,** 55—69

Sachs L. (1984): Applied Statistics. A Handbook of Techniques. Springer, New York

Salzberg B. M., Bezanilla F. (1983): An optical determination of the series resistance in *Loligo*. J. Gen. Physiol. **82,** 807—817

Schadow R. (1934): Die Darstellung von Resonanzkurven durch den Kathodenstrahloszillographen. Funktechn. Monatshefte No. 3, 105—109

Schumann H. (1980): Kompensation der elektrischen Auswirkungen des perinodalen Zugriffswider-

standes bei Ionenstrommessumgen am Ranvierschen Schnürring. Thesis, University of Kiel
Schumann H., Koppenhöfer E., Wiese H. (1983): Compensation of the low-pass filter properties of the current measuring internode in potential-clamped myelinated nerve fibres. Gen. Physiol. Biophys. **2,** 287—295
Sigworth F. J. (1980): The variance of sodium current fluctuations at the node of Ranvier. J. Physiol. (London) **307,** 97—129
Sommer R.-G., Schumann H., Koppenhöfer E. (1982): Changes in myelinated nerve fibres caused by insulating layers. Acta Physiol. Scand. **114,** 413—417
Stämpfli R., Hille B. (1976): 1. Electrophysiology of the Peripheral Myelinated Nerve. In: Frog Neurobiology (Eds. R. Llinás, W. Precht), pp. 3—32, Springer, Berlin
Steinmetz M. (1979): Ein Verfahren zur Messung von Ionenströmen an markhaltigen Nervenfasern — Seine Anwendungen und Grenzen. Thesis, University of Kiel
Steinmetz M., Sommer R.-G., Koppenhöfer E., Braak E. (1980): An inappropriate method to voltage clamp Ranvier nodes. Pflügers Arch. **384,** R30
Tietze U., Schenk C. (1986): Halbleiterschaltungstechnik. Springer, Berlin
Thomason J. G. (1955): Linear Feedback Analysis. Pergamon Press, London
Tuszynski A. (1989): Die Natriumstrom-Spannungskurve des Ranvierschen Schnürrings. Thesis, University of Kiel
Vogel W. (1974): Calcium and lanthanum effects at the nodal membrane. Pflügers Arch. **350,** 25—39
Waxman S. G. (1985): Structure and function of the myelinated fiber. In: Handbook of Clinical Neurology (Eds. P. J. Vinken, G. W. Bruyn, H. L. Klawans, J. C. Koetsier) Vol. **47,** pp. 1—28, Elsevier, Amsterdam
Wiese H., Duchâteau R. (1984): Measurement of absolute membrane potential with the potential clamp system of Nonner. Gen. Physiol. Biophys. **3,** 511—512
Wiese H., Koppenhöfer E. (1983): On the capacity current in myelinated nerve fibres. Gen. Physiol. Biophys. **2,** 297—312
Wiese H., Koppenhöfer E. (1988): Minimizing the influence of the series resistance in potential clamped Ranvier nodes. Gen. Physiol. Biophys. **7,** 143—156
Zaciu C., Tripsa M., Vasilescu V. (1981): Computer simulation of the effect of the nodal gap resistance on ionic current measurements in the Ranvier node membrane. Biophys. J. **36,** 797—802

Final version accepted May 2, 1989